JOURNAL OF MATERIALS SCIENCE 27 (1992) 226–232

Structure morphology effect of Ti and Nb stabilized austenitic stainless steel welds on corrosion properties

N. SARAFIANOS
Department of Mechanical Engineering, Laboratory of Physical Metallurgy, Aristotelian University, 54006 Thessaloniki, Greece

In this preliminary study the microstructure morphology of the austenitic stabilized stainless steel deposited by manual metal arc (MMA) welding on corrosion has been investigated as part of a study attempting to establish a quantitative correlation between the morphology and corrosion properties. It was found that corrosion resistance of the developed complex microstructure depends on the particular structure morphology at the parent metal-weld bead interface. For a given composition, the developed morphology is controlled by the interrelated parameters of heat input, cooling rate and joint geometry. Extensive precipitation of δ-ferrite results in a significant reduction of corrosion resistance.

1. Introduction

In the vast majority of applications demanding high performance steel grades under service conditions of stress, corrosion or high temperature, stainless steel is the most suitable [1–4]. In particular austenitic stainless steel grades are widely used in aggresive environments, or where high reliable standards are required such as chemical process plants, electricity supply industry and nuclear installations.

Although it was recognized about 30 years ago that grain boundary carbide precipitation render austenitic stainless steels susceptible to inter-granular corrosion [5–8] by depletion of dissolved chromium within the grain boundary [9], different opinions are held regarding the importance of ferrite precipitation in welding structure, with respect to, the reduction of the susceptibility to solidification cracking [10–15]. In determining the sensitivity to fissuring several controllable parameters should be considered, but control of the mode of solidification is more important [16–18]. One way of improving the joined engineering construction's performance is by adjusting the microstructure morphology which exhibit considerable variations through the process parameters. So, depending upon the grade of the particular steel used, the precipitation of a small amount of δ-ferrite between 3–8% fulfil this requirement.

This problem has been highlighted by many investigators [10–11, 14, 19, 20], but there is still room for research and improvement since many questions are still unanswered. In the course of this study investigating the effect of δ-ferrite on corrosion resistance of the multi-pass welded steel of the 321 and 347 AISI types, the aim was two-fold:

1. To account for the reasons why δ-ferrite is extensively precipitated and evenly distributed only throughout one of the earlier passes.

2. To deduce the effect of this selectively precipitated δ-ferrite on corrosion resistance of the multipass weld stabilized austenitic stainless steel being exposed to vapours of the hydrochloric solution for six months.

2. Experimental procedure

Austenitic stainless steel of grades 321 and 347 according to AISI standard, were selected in the form of plates 40 cm × 25 cm × 2.5 cm and two V welds were prepared by MMA welding process. The electrode used, according to AWS classification, was ER 347. An initial preheating of the electrodes was performed for 0.5 h at 350 °C, whilst the base metals were heated at 175 °C for 20 min. The heat input for all the weld passes was 1.8 kJ mm^{-1}. The chemical composition of both the parent metals and the filler metal are shown in Table I.

The actual carbon composition of the electrodes was between the upper and the lower bounds of the corresponding specifications of these grades. Two sections from each weld were used for macro–micro examination and Fig. 1 indicates the details of the welds.

3. Results and discussion

3.1. Microstructure

Fig. 1b shows the macrostructure of a weld cross-section. The passes are clearly distinguished and numbered in sequence while the arrows indicate the regions where the microstructure was examined in detail. Since the prime concern of this study was the establishment of a correlation between the corrosion resistance and the level of δ-ferrite present in the weld, attention was paid to the distribution and the morphology of ferrite. The factors which contribute to the

0022–2461/92 $03.00 + .12

TABLE I Chemical composition of the materials used

Material	C	Cr	Ni	Mo	Ti	Nb	Mn	Si	P	S	Cu	Fe
AISI 321 as-received in plate	0.09	18.2	9.95	–	0.82	–	1.24	0.67	0.007	0.018	–	Balance
AISI 347 as-received in plate	0.055	19.3	11.4	–	–	0.48	1.45	0.81	0.027	0.021	–	Balance
Electrode	0.062	19.3	9.51	0.68	–	–	0.65	0.71	0.035	0.027	0.32	Balance

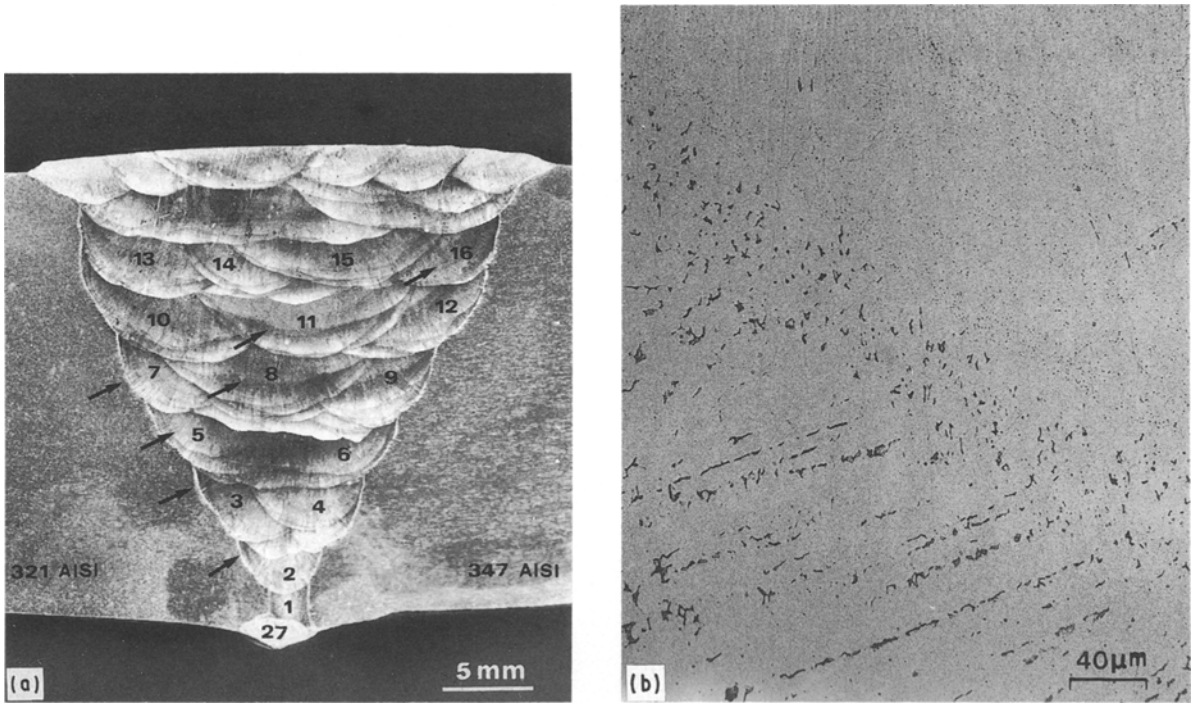

Figure 1 (a) Cross-section of the multi-pass weld after etching. Numbers indicate the run sequence of deposits; (b) massive precipitation of δ-ferrite observed on pass number 2.

complex morphology have been extensively developed in the literature [11, 15–17, 20], but the two which are believed to play an important role are: (a) the chemical composition and (b) the cooling rate, both of which strongly affect the microstructure morphology.

The amount of δ-ferrite present throughout the weld structure was determined at a level less than 0.8%. On the weld pass number 2 however, the amount of δ-ferrite was increased at $\sim$ 10%. Optical micrographs revealed a dense but discontinuous network of vermicular ferrite in this pass (Fig. 1b).

A transient of δ-ferrite morphology is observed on moving from the weld root region to the upper weld. So, a vermicular δ-ferrite is observed at the weld root region, and becomes more "blocky" or "lathy" towards the surface weld. Fig. 2a shows the microstructure of the weld root pass with a clear network of austenitic cellular subgrains and vermicular δ-ferrite at the austenitic subgrains boundaries. Fig. 2b was taken from pass number 2 and shows that columnar grains with δ-ferrite still of vermicular morphology occurring at austenitic grains, but the majority of δ-ferrite is observed at subgrain boundaries.

In the fusion zone the materials exhibit an epitaxial growth perpendicular to substrate growing on the planar grains which first developed upon the substrate. The morphology of δ-ferrite is vermicular and remains so throughout the fusion zone. Nucleation occurs both, at austenitic grains and subgrain boundaries (Fig. 3a), but retained ferrite is evidenced due to melting and solidification of the stagnant boundary layer when the dissipated superheat from liquid metal causes melting of the adjacent base metal (Fig. 3b).

Since a number of passes were made before the weld was completed, the whole microstructure consists mainly of as-deposited structure with columnar grains in the direction of high rate heat extraction, while a coarse grained zone was observed next. Finally a fine grain size zone was obtained due to the heat which each deposit was subjected to from the followed pass. Attention was drawn at the fine grain reheated zone where a more dense vermicular network of δ-ferrite was observed (Fig. 4). In the coarse grain regions away from the weld root, where as-deposited (casting) structure was obtained, the morphology of ferrite gradually changes to lathy or blocky, though in the near refined zone the remaining δ-ferrite has the vermicular morphology. The structure was derived from the solidification characteristics by reference to the *pseudo*-binary diagram Fe–Cr–Ni in the vertical section at

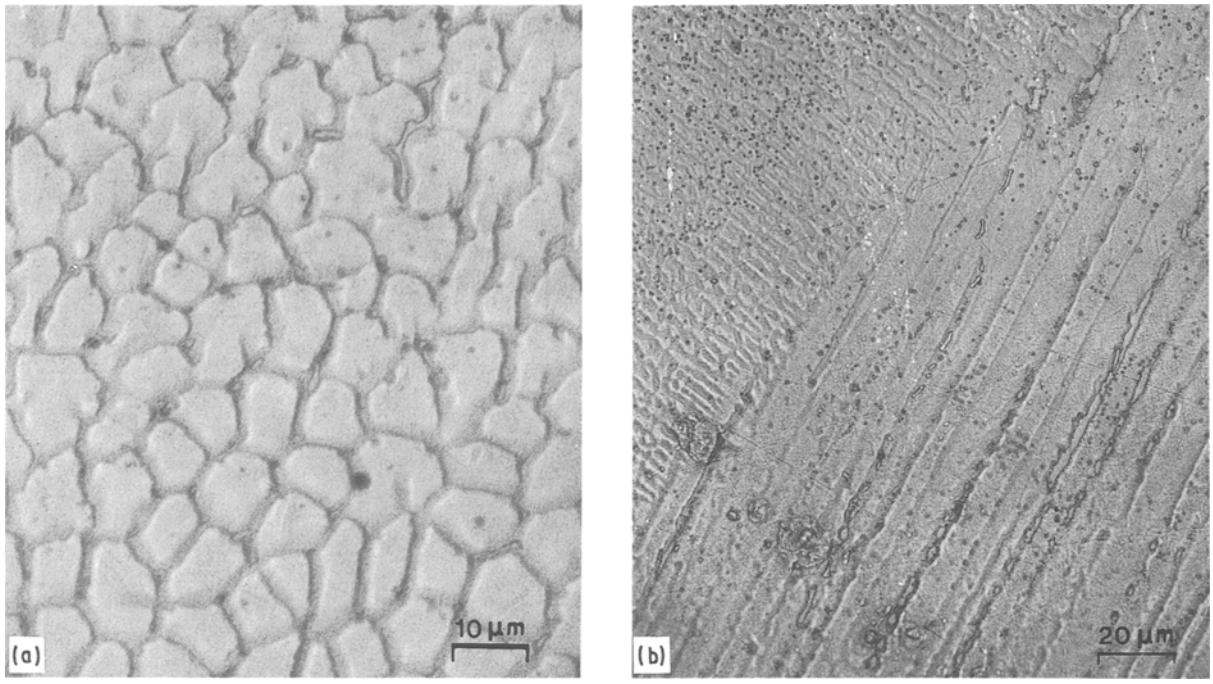

Figure 2 Optical micrographs showing: (a) austenitic subgrain cellular structure; (b) vermicular δ-ferrite mostly at subgrain boundaries with lathy σ-phase.

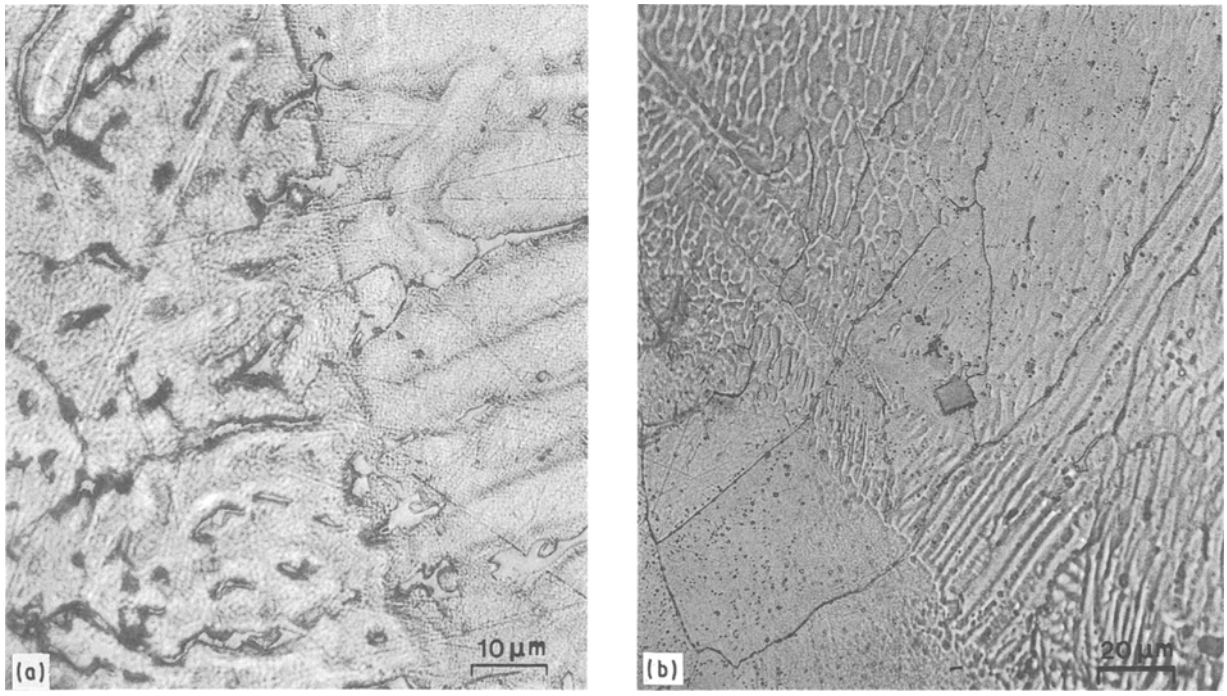

Figure 3 Microstructure at the base metal–weld bead interface showing: (a) epitaxial growth; (b) retained ferrite at subgrain boundaries.

60% Fe. Since the weld solidification is initially epitaxial, the first phase formed is, in fact, determined by the structure of the base metal at melting point. Assuming this to be austenitic, duplex structure is expected to develop during the transition from planar to cellular growth stage.

While it is very difficult to establish an acceptable agreement for the published data pertaining to the kinetics of δ-ferrite to austenite transformation, the findings of the structure morphology are in agreement, at least in a quantitative sense, with the results of other investigators. Although Kuwana and Kokawa [21] found a strong dependence of δ-ferrite morphology on the location of the weldment with high ferrite content on the bead surface and lower near the fusion boundary, they accept that local differences in both the content and morphology of δ-ferrite depend on the alloying and the cooling rate.

3.2. Cooling rate

The significance of the cooling rate on microstructure

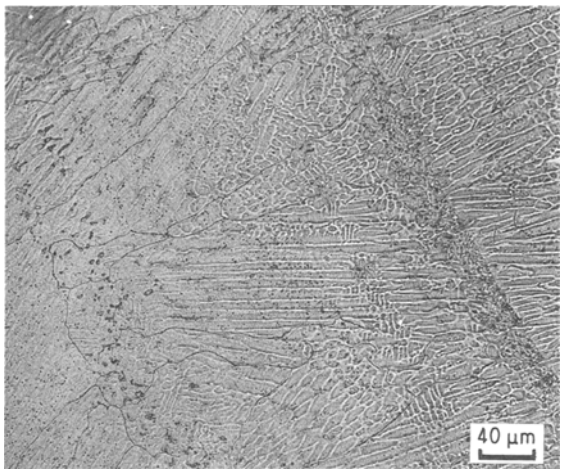

Figure 4 Microstructure of an interpass weld region showing an increased amount of δ-ferrite in the fine grain region.

has been well documented in the literature. So, detailed information on the temperature variations that a material experiences during welding is of considerable metallurgical importance, particularly when the welding of stabilized austenitic steel is concerned.

In attempting to calculate the actual cooling rate during welding, several factors must be considered. The temperature at any weld location is a function of the heat input, the thermal and physical properties of the materials used, the joint geometry and the actual temperature of the material due to the previous runs made during welding.

The solidification microstructure, and the corrosion properties of both, the weld zone and the HAZ are determined primarily by the cooling rate at the actual critical temperature corresponding to the liquid–solid and solid–solid transformations. However, obtaining reliable information about the cooling rate over the wide temperature range of the welding process, encounters unsurpassable difficulties when trying to obtain actual experimental measurements of cooling rate. A more realistic approach could be based on the temperature approximation wherever possible. In the fusion zone, where the actual thermal cycle can be accurately described due to the simple geometry, rather steady-state cycle conditions are imposed. So, in this zone the materials have an epitaxial growth starting at the initial solid–liquid interface towards the weld pool and form crystals of favourable orientation. Apart from this, a narrow planar zone was developed along the fusion line. A comprehensive understanding of the microstructure observed can be gained by considering both, the thermal gradient and the solidification rate. The content and morphology of δ-ferrite is then understood as the optimum condition of these two factors with respect to *pseudo*-binary Cr–Ni system. The rate of thermal gradient against solidification rate can be considered in terms of: (a) temperature profile estimated for a given cooling rate and, (b) determination of the solidification front moving towards the weld pool. Difficulties in calculating the cooling rates on the basis of the terms considered, have orientated the effort towards making a rough approximation of the thermal cycle. Since there is significant temperature fluctuation and gradual temperature rise, the material experiences a multi-pass welding alternation of melting and solidification.

It is interesting to see the interface reaction base metal–liquid. As the liquid metal is being deposited, the temperature gradient is initially high at the particular location under consideration and the angle between the normal to the base metal and the crystal growth direction ϑ is low, so, an epitaxial growth from the substrate occurs with an initial development of planar growth at the fusion line. As the thickness of the solidified material builds up the gradient decreases and the angle ϑ also decreases. Constitutional supercooling, therefore occurs, resulting in a transition from planar to cellular growth. Since this transition accounts for the ferrite morphology it is worthwhile to examine it in more detail. At the planar surface the first protrusion formed causes the solute Cr to be rejected laterally. This lowers the solidification temperature and triggers the formation of other protrusions which eventually grow almost parallel to the direction of maximum heat flow. The Cr rejected from the solidifying liquid concentrates between the cell walls which then solidify at lower temperatures. While the tips of the cells continuing to grow into the warmer melt are less enriched with Cr the resulting intercellular solute enrichment is due to the interaction between the temperature gradient, the cell shape and solute segregation. The important factor in determining the degree of segregation, particularly in stainless steel is the total amount of solutes present. The beneficial effect of the promoted duplex structure ($\alpha + \gamma$) reduces the susceptibility to hot cracking because of the increased fine dispersion in the phase boundary of δ-ferrite.

In view of the dependance of δ-ferrite kinetics transformation on various parameters it is not surprising that published data differ so widely. However, Lippod and Savage [22 and 23] reported microstructure due to solidification mode shifting from one primary austenite to one of primary ferrite and the position of retained ferrite shifts from the grain boundary to subgrain cores, while Massalski *et al.* [23] have reported microstructural transitions, similar to this work, as function of both composition and cooling rate. Piatty and Vedani [24] studied microstructural variations produced by surface acoustic waves (SAW) of heavy thickness plates, and published results quite similar to this work since they observed epitaxial growth and regions of planar growth. In an attempt to explain the welding structure morphology they stressed the importance of the thermal gradient and the solidification rate.

3.3. Corrosion

The effects of heating up the stabilized austenitic stainless steels during welding on corrosion resistance were examined in relation to the structure morphology. Fig. 5a shows the results of corrosion in the fusion zone after the prepared specimens have been etched in 2% of hydrochloric solution for a short

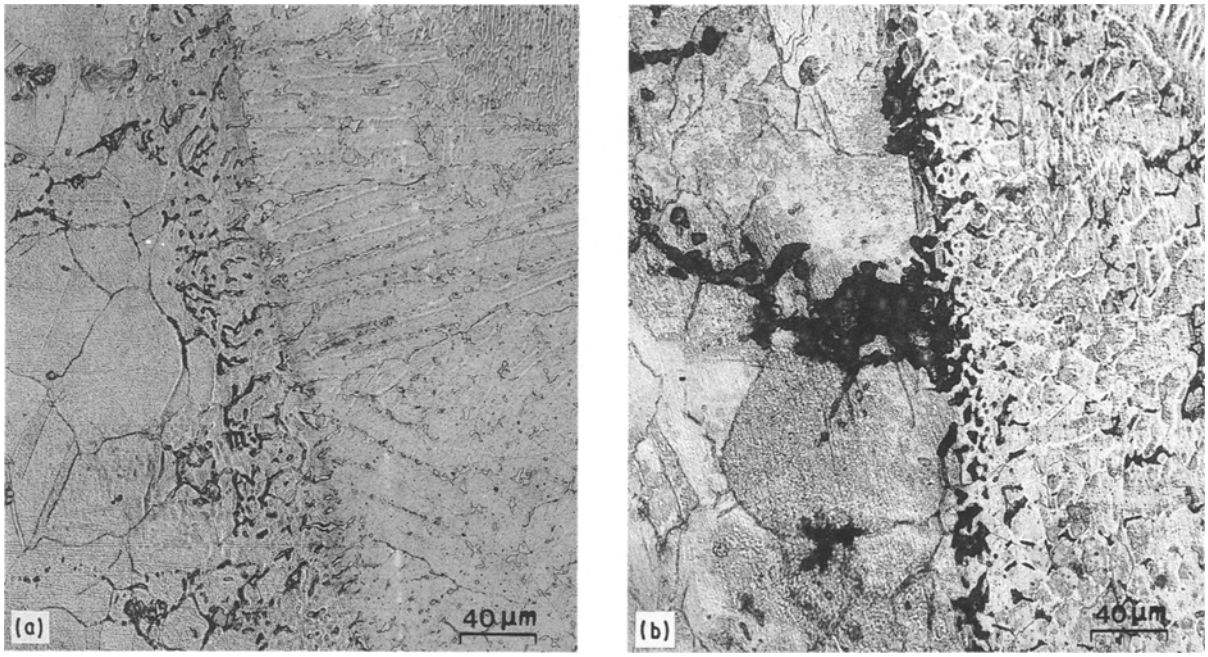

Figure 5 Optical micrographs at the HAZ of Ti stabilized steel after: (a) etching in 2% HCl solution; (b) exposure to solution vapours for a period of 183 days.

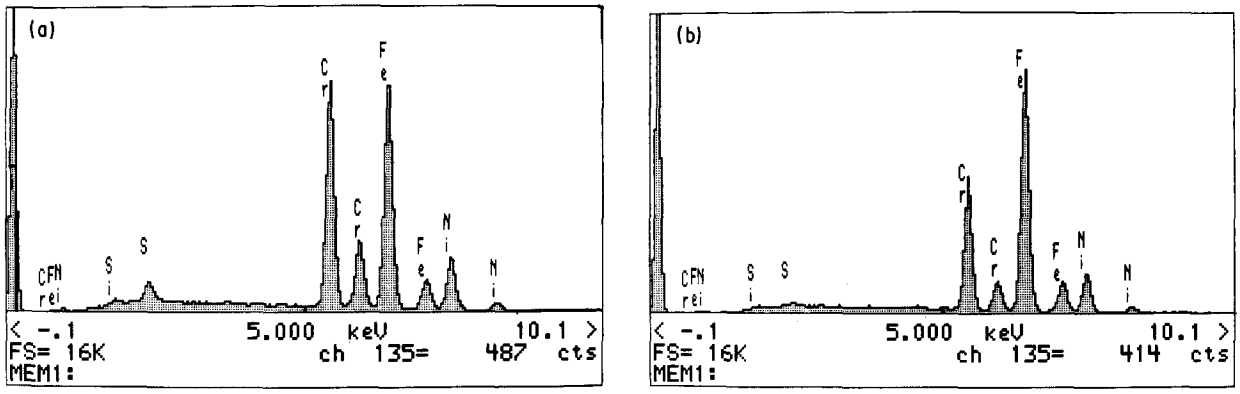

Figure 6 Typical EDS spectra of the Ti stabilized austenitic stainless steel 347 AISI type obtained from: (a) ferrite; (b) austenite.

period of time. Fig. 5b shows the corrosion at the fusion zone–HAZ interface under the same etching and after exposure to hydrochloric vapours for a period of 183 days. These micrographs clearly indicate that a selective corrosion attack occurs at the grain boundaries in the HAZ. This should be related to selective dissolution occurring at the grain boundary, and means inhomogenity primarily causes the intergranular attack. This type of corrosion is generally attributed to the denudatition of dissolved chromium within the grain boundaries and has usually been observed in the HAZ of stainless steel welding. Such a process involves temporary heating at high temperature as liquid metal is being deposited, and hence a varying thermal gradient is set up as the temperature dissipates through the parent metals. At the temperature range 550–850 °C chromium carbides precipitate at the grain boundary thus depleting them from chromium, rendering grain boundaries susceptible to corrosion. Since the base metals are Ti and Nb stabilized steels, respectively, and the electrode used was chosen to balance the composition, Cr remains contributing to the corrosion resistance of the steel. The greater affinity of C to Nb and Ti [25] with respect to Cr leads to stabilization of the structure, a well known phenomenon today, so selective corrosion at grain boundary should not be the case.

A detailed examination of the addressed problem requires the knowledge of a quantitative relationship of the stabilized elements regarding the C content as well as the actual structure and the transformation occurring on the basis of the phase diagram in order to acquire an understanding of the corrosion behaviour of the weld. With respect to the composition of 321 steel grade, Ti is balanced to C on the basis of stoichiometric composition to combine together leaving Cr free at grain boundaries. However, the full potential of titanium carbide formation largely depends on the solubility limit. This is the function of the solution heating temperature and if the carbon content slightly exceeds the solubility limit, apart from titanium carbide formation at higher temperature, Cr

carbides precipitate at progressively lower temperatures. The situation is deteriorated due to abnormal thermal cycles in the multi-run welding process as the number of passes is increased.

It is worth mentioning here that the intergranular attack observed was developed in the HAZ region corresponding to the particular pass where massive δ-ferrite occurred. This leads to the conclusion that selective corrosion is associated to retained ferrite at room temperature thus, giving rise to a selective solution at austenite–ferrite boundaries.

Fig. 6 shows the typical energy dispersive spectroscopy (EDS) spectra obtained from both the δ-ferrite and austenite. Comparison of the corresponding peak heights of the encountered elements Cr,Fe,Ni revealed that δ-ferrite is richer in Cr and to a lesser extent in Ni with respect to the γ-phase. The content of S was also found to be increased in the δ-ferrite as well as the Si content though at a lower level. The detrimental effect of S has long been reviewed but due to the spatial resolution of the electron beam (~ 3 μm) it was not possible to establish transient regions of compositional variation across the ferrite–austenite boundary. The non-coherency of δ-ferrite to austenite is clearly observed in Fig. 7a. This is due to different thermal expansion coefficients between ferrite–austenite [26]. On cooling, the primary δ-ferrite transforms to austenite and thermal stesses tend to be developed, resulting in decohesion. Thus the tendency to hot cracking is reduced. However, stress relief at the δ–γ interface leaves cavities associated with the σ-phase formation, hence cracking is initiated there. Fig. 7b shows the difference in structure morphology between δ-ferrite and σ-phase. Under the thermal cycles imposed by the welding passes, the presence of δ-ferrite accelerates the σ-phase formation. Due to higher Cr content in δ-ferrite it is where σ-phase growth is first observed. The growth of σ-phase depletes the austenitic matrix of Cr, Mo and Ti at the expense of δ-ferrite. This destabilizes the carbide growth, although it does not disappear. Microcracking in the HAZ which is always associated with the grain boundary where σ-phase nucleates and grows at the rate of δ-ferrite transformation, such regions are susceptible to corrosion. Scanning electron microscopy (SEM) analysis of such small particles indicated in Fig. 7b have been identified as titanium carbon nitrides. Fig. 8 shows the EDS analysis of a small particle indicated in Fig. 7b.

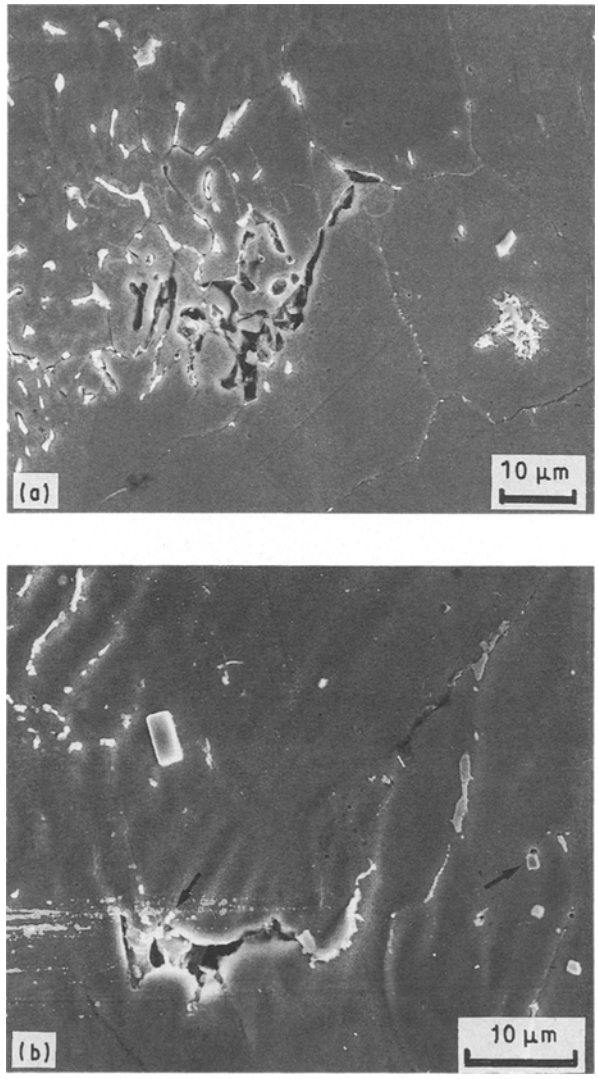

Figure 7 SEM micrographs from fusion zone showing: (a) transition of ferrite to σ-phase; (b) cracks associated with grain boundaries and σ-phase.

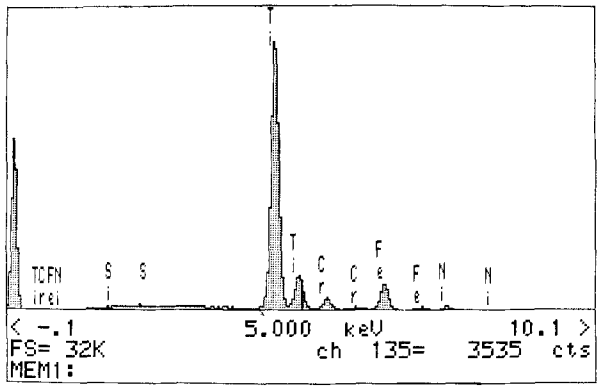

Figure 8 EDS analysis of the particle indicated in Fig. 7b.

References

1. C. STAWSTROM and M. HILLERT, *J. Iron Steel Inst.* (1969) 77.
2. H. E. HANNINEN, *Int. Met. Rev.* **3** (1973) 85.
3. G. F. SLATTERY, S. R. KEOWN and M. E. LAMBERT, *Metals Tech.* **10** (1983) 373.
4. E. P. BUTLER and M. C. BURKE, *Acta Metall.* **34** (1986) 557.
5. D. J. CHASTELL, P. DOIG, P. E. J. ELEWIT, and P. J. NORMAN, *Metall. Trans. A*, **19** (1988) 1445.
6. C. L. BRIANT, *ibid.* **10** (1979) 181.
7. C. L. BRIANT, R. A. MULFORD and E. L. HALL, *Corrosion*, **38** (1982) 468.
8. P. POZINAK and D. ELIEZER, *J. Mater. Sci.* **21** (1986) 3065.
9. J. M. LEITNAKER, *Welding J.* **61** (1982) 9.
10. F. MATSUDA, H. NAKAGAWA, T. UEHARA, S. KATAYAMA, and Y. ARATA, *Trans. JWRI*, **8** (1979) 17.
11. V. P. KUJANPAA, N. J. SUUTALA, T. K. TAKALO, and T. J. I. MOISIO, *Metal. Construct.* **12** (1980) 27.
12. Y. K. NIKOLAEV *et al.*, *Welding Prod.* **26** (1979) 47.
13. F. C. HULL, *Welding J.* **46** (1967) 399.
14. G. A. CLARK and P. GUHA, *Metal Construct.* **13** (1981) 12.
15. J. A. BROOKS, A. W. THOMSON, and J. C. WILLIAMS, *Welding J.* **63** (1984) 71.

16. T. TAKALO, N. SUUTALA, and T. MOISIO, *Metall. Trans. A*, **10** (1979) 1173.
17. M. J. GIESLAK, W. F. SAVAGE, *Welding J.* **60** (1981) 131.
18. S. A. DAVID, J. M. VITEK, and T. L. HEBBLE, *ibid.* **65** (1987) 289.
19. A. A. BUKI, A.YU IKONNIKOV, S. V. KOKHAN, V. V. GEIMUR, V. B. CHIZHOV, I. G. NOSKOV, and L. I. TYUL'PA, *Auto. Welding*, **November** (1985) 22.
20. T. P. S. GILL, M. VIJAYALAKSHMI, J. B. GNANAMOORTHY and K. A. PADMANABHAN, *Welding J.* **65** (1986) 122.
21. J. C. LIPPOLD and W. F. SAVAGE, *ibid.* **58** (1979) 362.
22. *Idem, ibid.* **59** (1980) 48.
23. T. B. MASSALSKI, J. H. PEREPEZKO, and J. JAKLOUSKY, *Mater. Sci. Eng.* **18** (1975) 193.
24. G. PIATTI, and M. VEDANI, *J. Mater. Sci.* **24** (1989) 1429.
25. B. AARONSON, in "Steel Strengthening Mechanisms", (Climax Molybdenum Co., 1968).
26. C. J. SMITHELLS, in "Metals Reference Book," (Butterworths, London, 1976) p. 966.

Received 3 September 1990
and accepted 28 February 1991